On the translational dynamics of bubbles in lithotripsy

Claus-Dieter Ohl
Department of Applied Physics, TU Twente
Postbus 217, 7500AE Enschede, The Netherlands

Lithotripsy, the medical use of strong acoustic waves, has become a major treatment method to disrupt kidney stones with the advantage of no need for surgery. In extra corporeal shock wave lithotripsy (ESWL) strong acoustic transients are generated either with piezo electrics or with an under-water spark discharge, and are applied to the patient by focusing them with an ellipsoidal reflector onto the kidney stone.

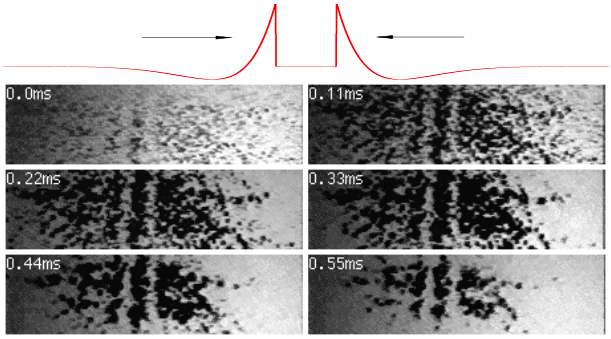

Fig. 1: Cavitation from two counter-traveling lithotripter waves. Top: The shape and directions of the pressure waves. Bottom: Six consecutive images taken at 9000 frames/s of the cavitation cloud produced. The field of view is $2 \times 7\,\mathrm{cm}^2$. Notice the pronounced structure of the cavitation zone with two vertical stripes with no activity. The central popualted area corresponds with the geometrical focus of both lithotripters (courtesy to D. Sokolav).

At least two different mechanisms have been proposed to be responsible for the destructive action [1]: the action of the acoustic wave inside and near the stone fracturing the stone by acoustics only. And as a second explanation: the destructive action from collapsing cavitation bubbles which are formed by the tensile part of the acoustic transient. The bubble collapse focuses its mechanical energy onto strongly localized spots on the stone surface. Also bubbles might migrate into the stone and fracture it during their expansion stage. A recent experiment from Bailey *et al.* [2] demonstrated that a "time inverted" lithotripter pulse which is hindering the growth of cavitation bubbles has much less ability to destruct the stone, compared to a standard pulse with the same magnitude of the positive and negative pressure amplitude. The author draws the conclusion that cavitation near the stone does support the stone fragmentation. However, cavitation can cause damage to the tissue and hemorrhage of the kidney, see for example [3]. Therefore, it is desirable to limit the cavitation area near to the stone. This paper discusses a method to control the size and shape of the cavitation area by considering the force acting on the bubbles causing a translational motion. The work was stimulated by the experimental results from D. Sokolov who presented the photographs (Fig. 1) of the cavitation zone generated by two counter-traveling lithotripter waves of the ASA 99 conference in Berlin.

Let us now model the bubble dynamics for two counter-traveling lithotripter pulses and deduce the force distribution near the focal center. To keep the calculations simple, a one dimensional model, and a *linear* superposition, $P(x,t) = P_1(x,t) + P_2(x,t)$, of the two lithotripter pulses traveling with opposite but constant speeds c are assumed:

$$P_{1,2}(x,t) = P_a e^{-\alpha(t\mp\frac{x}{c})} \cdot \cos\left(\omega(t\mp\frac{x}{c}) + \frac{\pi}{3}\right) \cdot \left(1+\tanh(n(t\mp\frac{x}{c}))\right) \quad . \tag{1}$$

The parameter n in the tanh–term in Eq. (1) allows for a non–zero rise time of the shock front. The following parameters have been used to model a commercial Dornier HM-3 system: $P_a = 410\,\mathrm{bar}$, velocity of sound $c = 1500$, $\alpha = 4.03\,10^5\,\mathrm{s}^{-1}$, $n = 10^8$, giving a rise time of 20 ns and an amplitude of 400 bar (the P_+/P_- ratio is 4.6). The bubble response is calculated with the Gilmore model assuming an adiabatic bubble content. Diffusion of gas has been checked to have no influence for the results presented and is therefore neglected.

The radiation pressure force, $\mathbf{F}$, acting on a bubble is given by $\mathbf{F}(x,t) = -\int \nabla p\, dV$. With the assumption that the pressure gradient is constant over the bubble volume this force can be equated with $\mathbf{F} = -\nabla p V$. When we consider the thickness of the shock front of typically $30\,\mu m$ in the calculations being in the order and less than the bubble volume, this assumption doesn't hold any more. Therefore, we estimate an effective gradient with the pressure difference on the two sides of the bubble divided by the bubble diameter:

$$F(x,t) = -\left[p(x+R,t) - p(x-R,t)\right] \cdot (2/3)\pi R^2(t) \quad . \tag{2}$$

From the experiment, see Fig. 1, a minimum bubble velocity can be deduced which is necessary to generate the two depletion areas of a length of 3 mm, and from the framing interval of 0.1 ms to be at least $\pm 15\,\mathrm{m/s}$. The velocity a bubble can reach by the action of the radiation pressure force from a single lithotripter pulse has been estimated from Church [4] to be up to 4 m/s. In the case of two counter-traveling lithotripter pulses this estimate doesn't hold anymore. The second pulse can act on a more expanded bubble leading to considerable higher forces.

The calculation of the force acting on the bubbles from two lithotripter pulses is straightforward: First the radial

bubble dynamics for different locations, x, in the focal area is calculated with the Gilmore model [4] driven by the pressure from Eq. (1). Then the time dependent force, $F(x,t)$, is obtained from Eq. (2). An example of the time evolution of the bubble radius, the pressure and the force is presented in Fig. 2 for $x = -3.7\,\mathrm{mm}$. Notice that the amplitude of the force from the second lithotripter pulse is three orders of magnitude larger than the force from the first one, which is not resolved in Fig. 2.

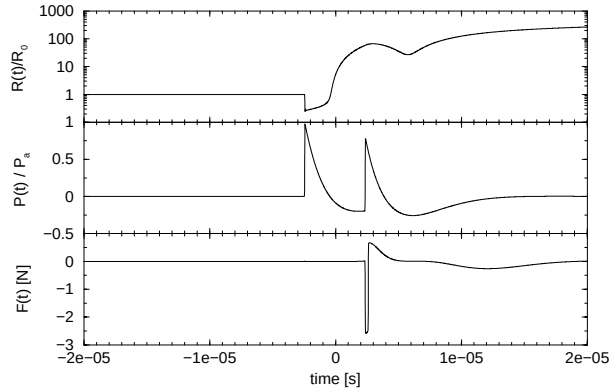

Fig. 2: Example of the bubble response, the time dependent pressure, and the instantenious radiation force for a bubble in the depopulated area of Fig. 1 at $x = -3.7\,\mathrm{mm}$ from the focus.

Figure 3 shows the maximum bubble radius, R_{max} and the time averaged force,$< F >$, as a function of the spatial coordinate x. The top curve of Fig. 3 clearly shows that the bubble expansion near the center is hindered but not diminished. Considering the radius of a half of that in the center, bubbles should be visible in Fig. 1. However, we find a strong dependency of $< F >$ on the spatial coordinate. From symmetry considerations the force in the center has to be zero and symmetric to the origin.

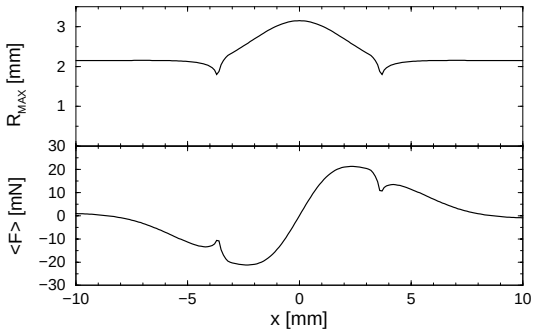

Fig. 3: *Top:* The maximum bubble radius, R_{max} after the passage of both lithotripter pulses in dependence on the spatial coordinate x. *Bottom:* The time averaged force, $< F >$ also in dependence on the spatial coordinate.

Bubbles at the center experience no force, the pressure acting on them is just double the pressure from a single pulse. For $x > 0$ bubbles will move to the right and for $x < 0$ they will move to the left. From conservation of the number of bubbles two regions left and right from the center with a depopulation will occur. Next to the depopulated area the pronounced gradients at $x = \pm 3.6\,\mathrm{mm}$ will result in two more highly populated regions. Further, at $x = \pm 4.2\,\mathrm{mm}$ the second local maximum (respectively, minimum) will result in a second less pronounced depopulated area. Finally a sign change of the force at $x = \pm 8.6\,\mathrm{mm}$ will localize the cavitation area as bubbles further away will be attracted towards the center.

All findings are in excellent agreement with the photographs. Even by a more careful inspection of Fig. 1 the second depopulated stripe as predicted by the calculations is visible. And finally, it was mentioned by Bailey[5], that with two lithotripters highly localized cavitation occurs, which agrees with the sign change of the force for larger distances from the center.

CONCLUSIONS

We have demonstrated that the pressure radiation force can explain the observed bubble distribution. For the sake of simplicity, no equation of motion for the bubbles has been applied. Experiments have to be performed to prove directly that the migration motion is responsible for the observed bubble distribution. With the help of the calculations presented we can estimate the observation area and timescale which have to be resolved in these future experiments. The time scale to be resolved has to be of the order of $1\,\mu\mathrm{s}$, the spatial resolution has to be at least $10\,\mu\mathrm{m}$ to localize the bubbles during the expansion stage. Further, it would be advantageous to track individual bubbles during the interaction with the lithotripter pulses. PIV and PTV have already been applied successfully in nanofluids where similar scales are present. Therefore, the author is confident that experiments on this issue will be performed and with further knowledge ESWL treatment, and especially the treatment of gall stones, will advance.

ACKNOWLEDGMENT

The author is thankful for the discussions with Dahlia Sokolov from APL (Seattle) and her permission to use the photographs in Fig. 1.

REFERENCES

1. W. Sass, M. Bräunlich, H.-P. Dreyer, E. Matura, W. Folberth, H.-G. Priesmeyer and J. Seifert, *The mechanisms of stone disintegration by shock wave*, Ultrasound Med. Biol. **17** 239–243 (1991).

2. M.R. Bailey, D.T. Blackstock, R.O. Cleveland, L.A. Crum, *Comparison of electrohydraulic lithotripters with rigid and pressure-release ellipsoidal reflectors. II. Cavitation fields*, J. Acoust. Soc. Am. **106** 1149-1160 (1999).

3. M. Delius, G. Enders, Z. Xuan, H.G. Liebich, W. Brendel, *Biological effects of shock waves: Kidney damage by shock waves in dogs — dose dependence*, Ultrasound Med. Biol. **14** 689-694 (1988).

4. C.C. Church, *A theoretical study of cavitation generated by an extracorporal shock wave lithotripter*, J. Acoust. Soc. Am. **86** 215–227 (1989).

5. M.R. Bailey, *Control of Acoustic Cavitation with Application to Lithotripsy*, Technical Report ARL-TR-97-1, University of Texas at Austin (1997).